Journal of Electroanalytical Chemistry 780 (2016) 249–256

Contents lists available at ScienceDirect

Journal of Electroanalytical Chemistry

journal homepage: www.elsevier.com/locate/jelechem

Photophysical, electrochemical, and quantum chemical properties of cationic iridium complexes with tunable emission color

Chozhidakath Damodharan Sunesh [a], Ramesh Kumar Chitumalla [b], Madayanad Suresh Subeesh [a], Kanagaraj Shanmugasundaram [a], Joonkyung Jang [b], Youngson Choe [a,*]

[a] Department of Polymer Science and Chemical Engineering, Pusan National University, Busan 609-735, Republic of Korea
[b] Department of Nanoenergy Engineering, Pusan National University, Busan 609-735, Republic of Korea

ARTICLE INFO

Article history:
Received 6 May 2016
Received in revised form 22 September 2016
Accepted 23 September 2016
Available online 24 September 2016

Keywords:
Iridium complex
Photophysical property
Electrochemical property
DFT calculation

ABSTRACT

We report the synthesis and characterization of the cationic iridium complexes $[Ir(ppy)_2(mpoxd)]PF_6$ (**1**), $[Ir(dfppy)_2(mpoxd)]PF_6$ (**2**), $[Ir(piq)_2(mpoxd)]PF_6$ (**3**), and $[Ir(pq)_2(mpoxd)]PF_6$ (**4**) bearing 2-phenylpyridine (Hppy), 2-(2,4-difluorophenyl)pyridine (Hdfppy), 1-phenylisoquinoline (Hpiq), and 2-phenylquinoline (Hpq) as cyclometalating ligands and 5-methyl-3-(2-pyridyl)-1,2,4-oxadiazole (mpoxd) as an ancillary ligand. UV–visible absorption spectra, photoluminescence (PL) emission spectra, and cyclic voltammetric measurements were obtained to explore the photophysical and electrochemical properties of **1**–**4**. Depending on the nature of the cyclometalating ligands, the complexes emit yellow-orange to blue light in acetonitrile solution at room temperature. The significant blue shift in the emission spectrum of **2** is due to the presence of electron-withdrawing fluorine atoms on Hdfppy, which stabilizes the highest occupied molecular orbital (HOMO) to a greater extent than in the other complexes. The electrochemical and photophysical properties of the complexes were also calculated using density functional theory (DFT) and time-dependent DFT simulations. The results indicate that the optical properties of the complexes can be effectively tuned by selective design of the cyclometalating and ancillary ligands.

1. Introduction

Ionic transition metal complexes (iTMCs) have attracted extensive interest due to their unique photophysical properties [1,2]. These materials have found application in photocatalysis [3], bioimaging [4], solar cells [5], light-emitting electrochemical cells (LECs) [6–9], and organic light-emitting diodes (OLEDs) [10]. Recently, LECs incorporating iTMCs have emerged as promising lighting devices and constitute an alternative to sophisticated organic light-emitting diodes (OLEDs) due to their low cost of production [11]. LECs are simpler devices than OLEDs and consist of a single ionic light-emitting layer processed from solution and placed between two metal electrodes by facile spin coating or printing processes [1]. LECs are also insensitive to the electrode work function and do not require air-sensitive charge injection layers, which allows non-rigorous encapsulation of the devices [12]. These benefits make LECs a favorable electroluminescent device for next-generation, flat-panel displays and solid-state lighting applications.

iTMCs, which emit light by phosphorescence, exhibit outstanding photoluminescent quantum yields (PLQYs) in comparison to polymer-based materials, which emit photons from singlet states and thus have a maximum internal quantum efficiency of only 25% [13,14]. The ionic nature of iTMCs leads to solubility in most polar organic solvents or even aqueous media [15,16]. Moreover, iTMCs possess attractive excited state properties and show multiple stable oxidation states [17]. iTMCs with superior redox reversibility is required in LEC devices to transport holes and electrons. During device operation, mobile ions in the active layer of the LEC move toward the corresponding electrode under an external bias and assist the injection of holes and electrons from the anode and cathode, respectively. The transport and recombination of these charge carriers results in the emission of light at low operating voltages and leads to better power conversion efficiencies [11,12,18].

Among the reported phosphorescent iTMCs, cyclometalated iridium(III) complexes are considered the most efficient and versatile triplet emitters for LECs, because of their excellent thermal stability, tunable emission color, and relatively short excited state lifetime [19–26]. Cationic iridium complexes can be easily synthesized and purified with very high yields, even close to the theoretical yield. Their large ligand field splitting and strong spin-orbit coupling produces efficient intersystem crossing from the singlet excited state to the triplet manifold, which enhances quantum efficiency. Cationic iridium complexes have the general formula $[Ir(C^N)_2(N^N)]^+$, where C^N is an anionic cyclometalating ligand and N^N is a neutral ancillary ligand. By tailoring

* Corresponding author.
E-mail address: choe@pusan.ac.kr (Y. Choe).

http://dx.doi.org/10.1016/j.jelechem.2016.09.037
1572-6657/

the structures of the C^N and N^N ligands, the emission color of iridium complexes can be controlled over the visible spectrum from blue to red [26–28]. In the archetypical complex, $[Ir(ppy)_2(bpy)]PF_6$, the highest occupied molecular orbital (HOMO) is located on the phenyl rings of ppy and the iridium ion, whereas the lowest unoccupied molecular orbital (LUMO) is centered on the ancillary bpy ligand [9]. Thus, color tuning can be achieved by changing substituents on the cyclometalating ligand, which alters the HOMO energy, whereas changes on the ancillary ligand alter the LUMO energy [9].

Recently, iridium complexes have been modified to emit light in the blue region, because few blue emitters based on charged iridium complexes have been reported so far [6]. Moreover, white LECs can be constructed from a combination of blue- with green- and red-emitting iridium complexes [23]. Thus, the design of blue-emitting heteroleptic iridium complexes is highly desirable. One strategy is to attach electron withdrawing substituents such as —F, $—CF_3$, and $—SO_2R$ to the phenyl groups of cyclometalating ligands, which stabilizes the HOMO. The second tactic is to attach electron donating groups ($—NR_2$) to the ancillary ligands, which destabilizes the LUMO. Both approaches widen the HOMO-LUMO gap resulting in light emission in the blue region.

In this paper, we report the synthesis and photophysical and electrochemical properties of a series of cationic iridium complexes, $[Ir(ppy)_2(mpoxd)]PF_6$ (**1**), $[Ir(dfppy)_2(mpoxd)]PF_6$ (**2**), $[Ir(piq)_2(mpoxd)]PF_6$ (**3**), and $[Ir(pq)_2(mpoxd)]PF_6$ (**4**) by incorporating the ancillary 5-methyl-3-(2-pyridyl)-1,2,4-oxadiazole (mpoxd) ligand into dichloro-bridged iridium dimers containing the cyclometalating 2-phenylpyridine (Hppy), 2-(2,4-difluorophenyl)pyridine (Hdfppy), 1-phenylisoquinoline (Hpiq), and 2-phenylquinoline (Hpq) ligands, respectively. Photoluminescence (PL) emission spectra demonstrate that the emission color of the complexes can be systematically tuned from yellow-orange to blue by selective design of the organic ligands. We performed density functional theory (DFT) and time-dependent DFT (TDDFT) calculations on complexes **1**, **2**, **3**, and **4**. The experimental photophysical and electrochemical properties were confirmed by the computations.

2. Experimental section

2.1. Materials and methods

All reactants and solvents were purchased from commercial sources and used without further purification unless otherwise stated. ^1H and ^{13}C NMR spectra were recorded with a Varian Unity Inova 500 MHz FT-NMR spectrometer in CD_2Cl_2 with tetramethylsilane (TMS) as internal standard. Elemental analyses were performed with an Elementar Vario EL CHN elemental analyzer. Electrospray ionization mass spectrometry (ESI-MS) analyses were obtained on an Agilent Q-TOF 6530 MS/MS system using dichloromethane as matrix solvent. Absorption and photoluminescence (PL) emission spectra of the complexes (10^{-5} M) were measured in deaerated acetonitrile solution at room temperature using an Agilent 8453 spectrophotometer and an F-7000 FL spectrophotometer, respectively. The PLQYs were calculated in acetonitrile solutions with quinine sulfate ($\Phi p = 0.545$ in 1 M H_2SO_4) as the standard. The PL decay lifetimes were measured in acetonitrile solution using a compact photoluminescence lifetime spectrometer. The thin film PL spectra were made on quartz substrates by spin coating the complexes in acetonitrile solution (10^{-3} M) with a thickness of about 100 nm. The PL quantum yields of thin films were also calculated using 9,10-diphenylanthracene ($\Phi p = 0.90$ in cyclohexane) as the external reference. Cyclic voltammetry (CV) was performed using an Ivium potentiostat/galvanostat in acetonitrile solution (10^{-3} M). A 0.1 M solution of tetrabutylammonium hexafluorophosphate ($TBAPF_6$) served as supporting electrolyte. Potentials were referenced internally to the ferricenium/ferrocene (Fc^+/Fc) couple at a scan rate of 100 mV s^{-1}. The electrolytic cell consisted of a glassy carbon working electrode, platinum wire counter electrode, and Ag/AgCl reference electrode. The HOMO (E_{HOMO}) and LUMO (E_{LUMO}) energy levels and energy gaps (E_{gap}) of the iridium complexes were calculated from the oxidation (E_{ox}) and reduction (E_{red}) potentials using the empirical formulae [29,30]: $E_{HOMO} = [-e(E_{ox(vs.\ Ag/AgCl)} - E_{1/2(Fc+/Fc\ vs.\ Ag/AgCl))}] - 4.8$ eV, $E_{LUMO} = [-e(E_{red} - E_{1/2})] - 4.8$ eV, and $E_{gap} = E_{HOMO} - E_{LUMO}$, where $E_{1/2\ (Fc+/Fc\ vs.\ Ag/AgCl)}$ is the redox potential of ferrocene (0.43 V).

2.2. Synthesis of cationic iridium complexes

The iridium complexes were prepared by first isolating the μ–dichloro iridium (III) dimers described by Nonoyama by refluxing 1.0 eq of $IrCl_3 \cdot xH_2O$ with 2.3 eq of the cyclometalating Hppy, Hdfppy, Hpiq, or Hpq ligands in a mixture of 2–ethoxyethanol and water (3:1 v/v) for 24 h [31]. The $[Ir(C^N)_2(\mu\text{–}Cl)]_2$ dimers were then cleaved with mpoxd at 60 °C under argon for 18 h to form the monomeric complexes as chloride salts followed by anion metathesis using ammonium hexafluorophosphate, NH_4PF_6. The cationic $[Ir(C^N)_2(N^N)]PF_6$ complexes were obtained in good yield and characterized by ^1H NMR spectroscopy (ESI Fig. S1), elemental analysis, and mass spectrometry (ESI, Fig. S2). The synthetic steps with structures of the cyclometalating ligands and cationic complexes are shown in Scheme 1.

2.2.1. Synthesis of $[Ir(ppy)_2(mpoxd)]PF6$ (**1**)

$[Ir(ppy)_2Cl]_2$ (108 mg, 0.1 mmol) and mpoxd (37 mg, 0.23 mmol) were dissolved in dichloromethane (15 mL) and methanol (15 mL). The mixture was heated to reflux at 60 °C under argon for 18 h. The chloride solution of the complex was cooled to room temperature and subjected to ion exchange with solid NH_4PF_6 (65 mg, 0.4 mmol). The solvent was removed under reduced pressure after stirring for 1 h at room temperature. The residue was dissolved in dichloromethane and filtered to remove insoluble inorganic impurities. The complex was precipitated by the addition of diethyl ether to the filtrate, which was then filtered and dried in a vacuum oven for 24 h. The crude material was crystallized from an acetonitrile/diethyl ether mixture. Yield: 137 mg, 0.17 mmol, 85%. ^1H NMR (500 MHz, CD_2Cl_2) δ (ppm): 8.50 (d, J = 7.75 Hz, 1H), 8.21–8.14 (m, 1H), 8.01–7.95 (m, 4H), 7.88–7.83 (m, 2H), 7.76–7.70 (m, 2H), 7.60–7.56 (m, 1H), 7.52 (d, J = 5.11 Hz, 1H), 7.22–7.18 (m, 1H), 7.10–7.03 (m, 3H), 6.95–6.89 (m, 2H), 6.34 (d, J = 7.72 Hz, 1H), 6.26 (d, J = 7.62 Hz, 1H), 2.01 (s, 3H). ^{13}C NMR (126 MHz, CD_2Cl_2) δ (ppm): 168.3, 167.6, 151.9, 149.9, 146.6, 144.3,

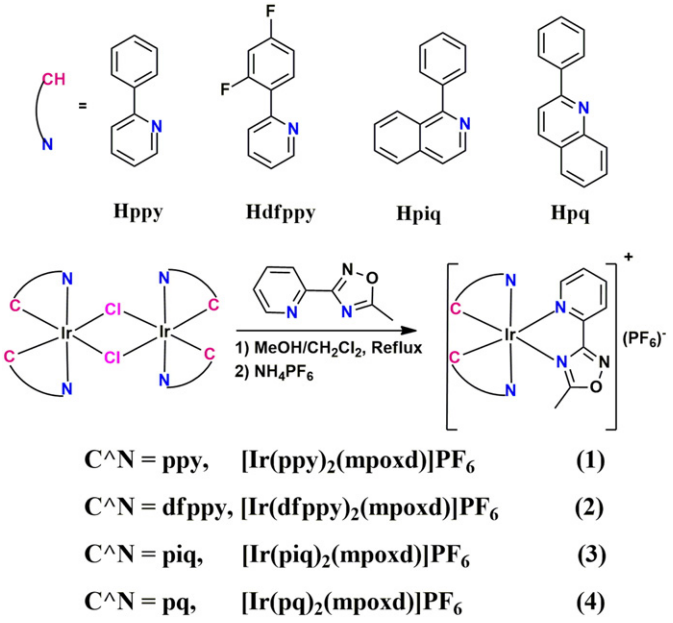

Scheme 1. Chemical structures of cyclometalating ligands and synthetic routes to complexes **1**–**4**.

139.2, 132.7, 131.8, 131.2, 126.3, 125.4, 123.7, 120.5, 11.8. Anal. Calcd (%) for $C_{30}H_{23}N_5OPF_6Ir$: C, 44.67; H, 2.87; N, 8.68. Found: C, 44.70; H, 2.86; N, 8.75. ESI-MS (*m/z*): 662.12 $[M\text{-}PF_6]^+$.

2.2.2. Synthesis of $[Ir(dfppy)_2(mpoxd)]PF_6$ (**2**)

The complex was prepared by the above procedure by replacing $[Ir(ppy)_2Cl]_2$ with $[Ir(dfppy)_2Cl]_2$ (122 mg, 0.1 mmol). Yield: 142 mg, 0.16 mmol, 81%. ^{1}H NMR (500 MHz, CD_2Cl_2) δ (ppm): 8.55 (d, J = 7.86 Hz, 1H), 8.37–8.33 (m, 2H), 8.28–8.20 (m, 1H), 8.07 (d, J = 5 Hz, 1H), 7.99–7.86 (m, 3H), 7.78–7.60 (m, 1H), 7.49 (d, J = 5.04 Hz, 1H), 7.30–7.27 (m, 1H), 7.17–7.13 (m, 1H), 6.67–6.63 (m, 2H), 5.77 (d, J = 8.37 Hz, 1H), 5.66 (d, J = 8.51 Hz, 1H), 2.21 (s, 3H). ^{13}C NMR (126 MHz, CD_2Cl_2) δ (ppm): 181.3, 169.7, 163.9, 160.9, 160.4, 151.7, 150.4, 141.2, 131.2, 126.7, 124.6, 117.1, 110.6, 12.3. Anal. Calcd (%) for $C_{30}H_{19}N_5OPF_{10}Ir$: C, 41.01; H, 2.18; N, 7.97. Found: C, 41.09; H, 2.14; N, 7.85. ESI-MS (*m/z*): 734.08 $[M\text{-}PF_6]^+$.

2.2.3. Synthesis of $[Ir(piq)_2(mpoxd)]PF_6$ (**3**)

The complex was prepared from $[Ir(piq)_2Cl]_2$ (127 mg, 0.1 mmol) and mpoxd (37 mg, 0.23 mmol). Yield: 144 mg, 0.16 mmol, 79%. ^{1}H NMR (500 MHz, CD_2Cl_2) δ (ppm): 8.99–8.94 (m, 2H), 8.54 (d, J = 7.80 Hz, 1H), 8.34 (d, J = 8.01 Hz, 1H), 8.29 (d, J = 8.01 Hz, 1H), 8.20–8.14 (m, 1H), 8.01–7.95 (m, 2H), 7.89–7.80 (m, 6H), 7.58–7.52 (m, 2H), 7.45–7.38 (m, 2H), 7.19–7.12 (m, 2H), 6.91–6.87 (m, 2H), 6.36 (d, J = 7.73 Hz, 1H), 6.21 (d, J = 7.67 Hz, 1H), 1.95 (s, 3H). ^{13}C NMR (126 MHz, CD_2Cl_2) δ (ppm): 180.9, 170.1, 168.9, 151.7, 149.8, 146.1, 144.3, 140.4, 137.9, 133.4, 130.2, 129.8, 129.6, 128.2, 127.4, 126.9, 126.4, 123.4, 122.9, 110.6, 11.5. Anal. Calcd (%) for $C_{38}H_{27}N_5OPF_6Ir$: C, 50.33; H, 3.00; N, 7.72. Found: C, 50.36; H, 3.09; N, 7.63. ESI-MS (*m/z*): 762.18 $[M\text{-}PF_6]^+$.

2.2.4. Synthesis of $[Ir(pq)_2(mpoxd)]PF_6$ (**4**)

This complex was prepared from $[Ir(pq)_2Cl]_2$ (127 mg, 0.1 mmol) and mpoxd (37 mg, 0.23 mmol). Yield: 140 mg, 0.15 mmol, 77%. ^{1}H NMR (500 MHz, CD_2Cl_2) δ (ppm): 8.38 (d, J = 8.60 Hz, 1H), 8.32 (d, J = 8.87 Hz, 1H), 8.25–8.17 (m, 3H), 8.07–7.96 (m, 4H), 7.85 (t, J = 8.12 Hz and 8.12 Hz, 2H), 7.64–7.58 (m, 1H), 7.56 (d, J = 8.83 Hz, 1H), 7.51–7.33 (m, 2H), 7.24–7.16 (m, 3H), 7.08–6.98 (m, 2H), 6.88–6.83 (m, 2H), 6.62 (d, J = 7.79 Hz, 1H), 6.56 (d, J = 6.77 Hz, 1H), 2.27 (s, 3H). ^{13}C NMR (126 MHz, CD_2Cl_2) δ (ppm): 180.7, 170.1, 169.6, 157.8, 151.7, 147.6, 144.4, 140.5, 137.9, 129.6, 128.2, 128.1, 127.5, 127.3, 126.9, 126.3, 123.4, 120.4, 118.6, 13.8. Anal. Calcd (%) for $C_{38}H_{27}N_5OPF_6Ir$: C, 50.33; H, 3.00; N, 7.72. Found: C, 50.35; H, 3.04; N, 7.79. ESI-MS (*m/z*): 762.18 $[M\text{-}PF_6]^+$.

2.3. Quantum chemical calculations

The calculations in this work were obtained using the Gaussian 09 ab initio/DFT quantum chemical program [32]. Geometry optimization and vibrational frequency analysis of the complexes were performed employing a hybrid B3LYP [33–35] exchange and correlation functional. We used 6-31G(d,p) basis functions for the H, C, N, O, and F atoms and a "double-ξ" quality basis set (LanL2DZ) and ECP [36–38] for the Ir atom. Theoretical singlet equilibrium structures were obtained when the maximum internal forces acting on all atoms and the stress were less than 4.5×10^{-4} eV Å^{-1} and 1.01×10^{-3} kbar, respectively. Minima were confirmed by the presence of all positive values in the harmonic vibrational frequency analysis. We simulated UV–vis absorption spectra with the pre-optimized structures using the TDDFT formalism. Acetonitrile solvent was mimicked by using the polarizable continuum model [39,40] in the TDDFT simulations. Phosphorescence emission data were obtained by the employing self-consistent-field energy difference (ΔSCF) method. The methods and basis sets used in this study have been shown to give reliable results for transition metal complexes [41].

3. Results and discussion

3.1. Synthesis and characterization

Cationic iridium complexes were synthesized by reaction of the corresponding dichloro-bridged iridium dimer, $[Ir(C\text{^}N)_2(\mu\text{–}Cl)]_2$, with 2.3 eq of mpoxd followed by ion exchange with NH_4PF_6. Purification of crude products gave the desired complexes, $[Ir(C\text{^}N)_2(N\text{^}N)]PF_6$, in good yields. The structures of complexes **1**–**4** are shown in Fig. 1. All complexes were fully characterized by ^{1}H NMR spectroscopy, elemental analysis, and mass spectrometry (see Experimental section and Figs. S1–S2).

3.2. Quantum chemical calculations

DFT and TDDFT studies are widely used to explain the experimentally observed electrochemical and photophysical behavior of transition metal complexes [42]. In this study, we performed DFT/TDDFT simulations of the four Ir complexes to gain insight into their structural, electronic, electrochemical, and photophysical properties. All complexes have pseudo-octahedral coordination geometry around the metal center. The optimized geometries of the complexes **1** and **2** are depicted in Fig. 2; those of complexes **3** and **4** are depicted in Fig. S3. The important geometrical parameters around the metal center are given in Table 1. The bond lengths between the carbon atoms of the cyclometalating ligands and Ir (Ir-C4/Ir-C5) in complexes **1** and **2** are slightly longer than those in complexes **3** and **4** and range from 2.001 to 2.019 Å. The Ir-N3/Ir-N6 bond distances in complexes **1**, **2**, and **3** equal approximately 2.085 Å, whereas these distances are elongated in complex **4** (ca. 2.13 Å). The distances of Ir—N bonds to the ancillary ligands are slightly longer and range from 2.243 to 2.276 Å in complexes **1**–**3** and from 2.313 to 2.316 Å in **4**. The phenylpyridine bond angles with Ir (N3-Ir-C4/C5-Ir-N6) are approximately 80° and do not change significantly from complex **1** to **4**. The ancillary ligand bond angles with Ir (N1-Ir-N2) are approximately 74°.

The Kohn–Sham orbitals of the four iridium complexes are displayed in Fig. 3. From the electron density distribution, it is clear that the highest occupied molecular orbital (HOMO) is localized mainly on the metal center and ancillary ligand and partly on the cyclometalating

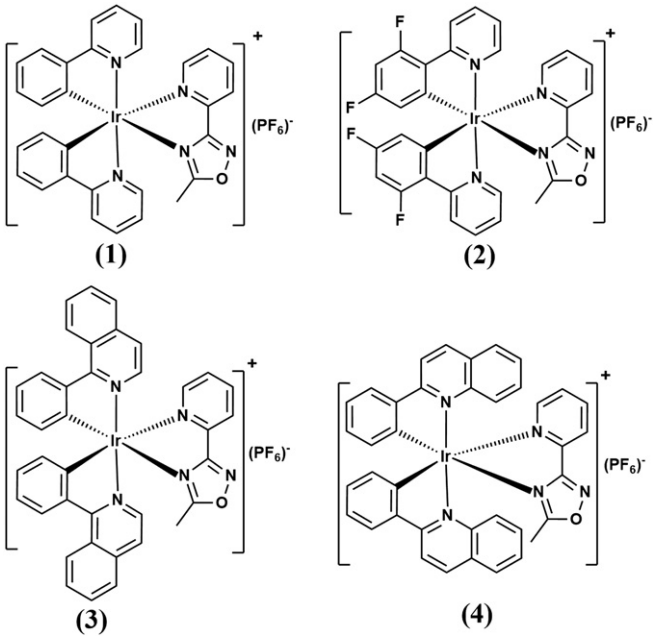

Fig. 1. Structures of heteroleptic iridium complexes **1**–**4** bearing the oxadiazole ancillary ligand.

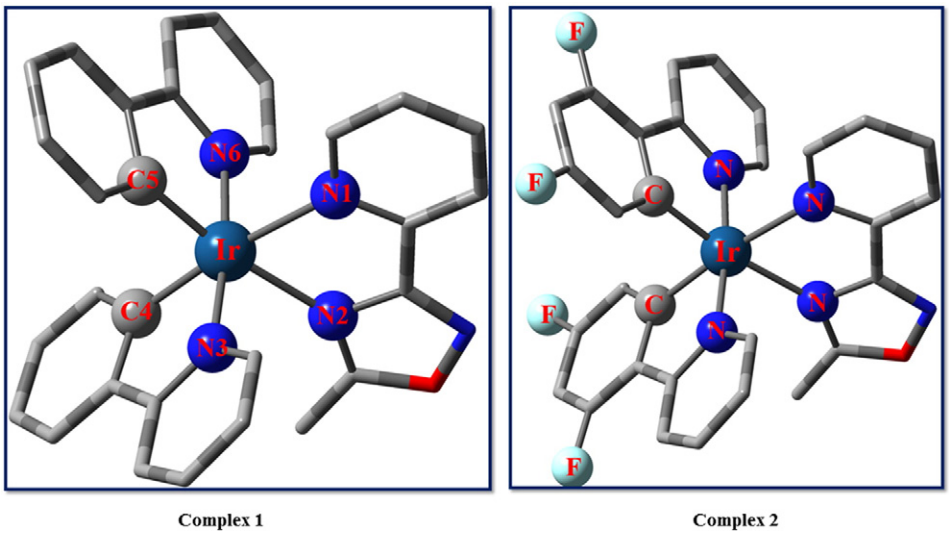

Fig. 2. Optimized molecular structures of complexes **1** and **2** obtained at the B3LYP/6-31G(d,p)/LanL2DZ level of theory. Hydrogen atoms are omitted for clarity.

ligands. The lowest unoccupied molecular orbital (LUMO) is localized mainly on the cyclometalating ligands and partly on the ancillary ligand. From the calculated HOMO and LUMO eigenvalues, it is evident that the HOMO and LUMO of complex **2** are stabilized relative to complex **1**. The HOMO and LUMO stabilization is attributed to the electron-withdrawing nature of the fluorine substituents. Stabilization of the HOMO energy in **2** explains the more positive oxidation potential (1.36 V) observed experimentally for this complex relative to that of **1** (1.04 V). Because complexes **3** and **4** do not vary structurally to a large extent, their HOMO and LUMO eigenvalues are similar. The HOMO, LUMO, and HOMO-LUMO difference energies of the four complexes (Table 2) are in excellent agreement with the electrochemical data obtained by CV. In this study, we calculated each LUMO energy by summing the HOMO energy and the corresponding first excitation energy.

Fig. 4 shows the simulated UV–visible absorption spectra of the four iridium complexes in acetonitrile and the corresponding photophysical data from Table 3. The TDDFT simulations reproduce the main bands observed in the experimental spectra. The most intense singlet transition in the low energy region is located at 395 and 369 nm for complexes **1** and **2** and at 460 and 451 nm for complexes **3** and **4**, respectively. These low energy absorptions are assigned to metal-to-ligand charge transfer (MLCT). The hypsochromic shift for complex **2** relative to **1** is arises from the increased HOMO-LUMO energy difference upon fluorine substitution of the cyclometalating ligands (vide supra). The absorption maxima in the high energy region arise predominantly from the HOMO to LUMO + 1 transition. Complexes **3** and **4** show a considerable bathochromic shift relative to complexes **1** and **2** in their absorption spectra. The most intense absorptions for **1** and **2** occur near 290 nm, whereas those for **3** and **4** fall beyond 320 nm. The intense transitions in the high energy region are assigned to ligand $\pi \rightarrow \pi^*$ charge transfers. The UV–visible absorption spectra and corresponding oscillator strengths of the four complexes and presented in Fig. S4. We employed the ΔSCF method to obtain the phosphorescence emission data given in Table 3. The phosphorescence emission maxima occur at 582, 565, 592, and 571 nm for complexes **1**, **2**, **3**, and **4**, respectively. The calculated emission values are in excellent agreement with the experimental data. The absorption and emission spectra are blue shifted on going from complex **1** to **2** and also from complex **3** to **4**.

Table 1
Important bond lengths (Å) and bond angles (degrees) for all four Ir complexes in their most stable conformations. The numbering of the atoms is shown in Fig. 5.

	1	2	3	4
Bond lengths				
Ir-N1	2.269	2.262	2.257	2.316
Ir-N2	2.253	2.243	2.276	2.313
Ir-N3	2.085	2.083	2.085	2.138
Ir-C4	2.019	2.017	2.007	2.007
Ir-C5	2.015	2.012	2.012	2.001
Ir-N6	2.084	2.083	2.086	2.133
Bond angles				
N1-Ir-N2	74.6	74.8	74.2	73.1
N3-Ir-C4	80.1	80.2	79.4	79.7
C5-Ir-N6	80.2	80.3	79.3	79.8

3.3. Photophysical properties

The photophysical properties of complexes **1**–**4** are summarized in Table 4 and shown in Fig. 5. The UV–visible spectra in Fig. 5 show broad and intense absorption bands in the high energy region from 200 to 300 nm. These bands are assigned to $^1\pi$—π^* ligand-centered (LC) transitions, which vary in energy due to the presence of different cyclometalating ligands. Less intense absorption bands at 300 to 400 nm are assigned to spin-allowed metal-to-ligand (^{1}MLCT) and ligand-to-ligand (^{1}LLCT) charge transfer transitions. Bands observed in the visible region beyond 400 nm are assigned to ^{3}MLCT, ^{3}LLCT, and LC $^3\pi$—π^* transitions of the complexes [43]. The spin-forbidden triplet transitions, which display substantial intensity, are partially allowed by mixing with the higher lying ^{1}MLCT transitions due to the strong spin-orbit coupling of the heavy iridium atom [44,45]. The absorption spectrum of **2** in the lower energy region is blue-shifted by 36 nm relative to that of **3** due to the presence of electron-withdrawing fluorine atoms on the cyclometalating ligand of the former complex. The extended conjugation of the cyclometalating ligands in complexes **3** and **4** shifts their absorption bands to longer wavelengths in the visible region.

PL emission spectra of the complexes were recorded in acetonitrile solution as shown in Fig. 6. The emission spectra display broad, structured and featureless peaks that range 421 to 621 nm and depend on the identity of cyclometalating ligand. The emission spectrum of **1** shows a broad band centered at 575 nm, which yields yellow emission. The featureless character of the band is indicative of emission from the ^{3}MLCT excited state [46,47]. It is noteworthy that complex **2** shows a strong blue emission with a maximum centered at 453 nm and shoulder peaks at 487 and 514 nm. Replacement of ppy by dfppy produces much more structured emission spectrum, which indicates that the emissive excited states of **2** have predominant LC $^3\pi_{(C\hat{}N)}$–$\pi^*_{(C\hat{}N)}$ character other than ^{3}MLCT or ^{3}LLCT characters [44,45,47–49]. The blue shift in the emission spectrum of **2** can be explained by the electron-withdrawing nature of fluorine atoms on the cyclometalating ligands. Electron-

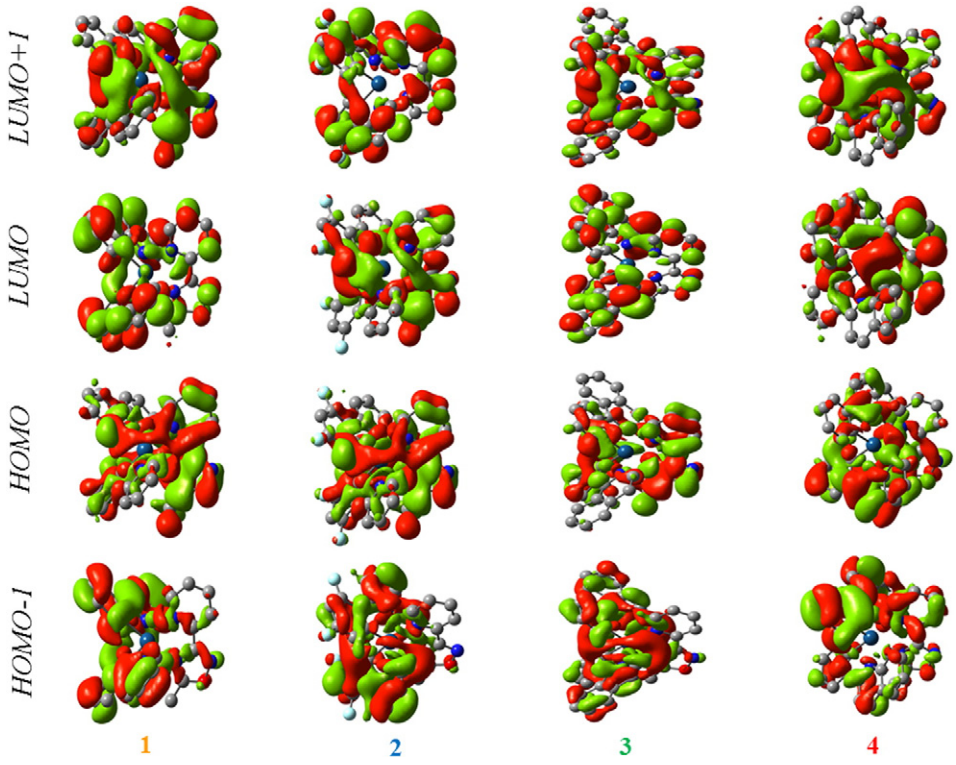

Fig. 3. The electron density distribution from HOMO-1 to LUMO + 1 for complexes **1–4** (isosurface: 0.02 e Å^{-3}) obtained from DFT calculations.

withdrawing substituents reduce the electron density on iridium and lower the HOMO energy level of **2**. Complex **3** likewise shows a structured emission profile, which indicates a similar emissive mechanism for the two complexes. The emission spectrum of **3** is red-shifted with a maximum at 589 nm and a shoulder at 621 nm in the yellow-orange region of the spectrum. The red-shift in the PL emission spectrum of complex **3** is due to the electron donating nature of isoquinoline moiety as a result of an increased π-conjugation, which leads to the destabilization of HOMO to large extent than complexes **1**, **2**, and **4.** The emission spectrum of **4** exhibits a sharp peak at 561 nm in the yellow region. The PL emission was blue shifted for complex **4** as compared to complex **3** due to the stabilization of the HOMO energy level as predicted by DFT calculations and thereby increase the energy gap between HOMO and LUMO energy levels.

In dilute acetonitrile solution, complexes **1–4** give PLQYs of 0.09, 0.12, 0.31, and 0.07, respectively. The excited state lifetime (τ) in degassed acetonitrile solutions are 34.63 ns, 44 ns, 0.51 μs, and 10.75 ns for complexes **1–4**, respectively (Fig. S5). The excited state lifetime of complex **3** is much longer than that of other complexes indicating the emissive excited state of complex **3** has pronounced LC ^{3}π–π* character [1,49]. For the further evidence of predominant ^{3}LC character of the T_1 excited state, the radiative decay rate constant (K_r) of the complexes was calculated from the experimental PLQY (Φ) value and excited state lifetime (τ), according to the equation $K_r = \Phi\tau^{-1}$. A smaller value of K_r usually designates a stronger LC character in the triplet excited state of complexes [49]. It is evident from the equation that the longer excited state lifetime of the complexes, smaller will be the K_r value, confirming a less pronounced ^{3}MLCT character of its emissive excited state. The calculated radiative decay rates (K_r) of complexes **1–4** are 2.83 × 10^6, 2.69 × 10^6, 0.61 × 10^6, 6.61 × 10^6 s^{-1}, respectively, whereas their respective nonradiative decay rates (K_{nr}) are 1.04 × 10^7, 2.0 × 10^7, 0.14 × 10^7, and 8.64 × 10^7 s^{-1}. The smaller Kr value of complex **3** thus affirms that the emissive excited state must have stronger LC ^{3}π–π* character [49].

The PL emission spectra of complexes **1–4** in neat films is shown in Fig. 7. The PL spectra of complexes in neat film are almost identical to those in solutions. Compared with their solution spectra, the PL spectra in neat films of all the complexes are significantly red shifted to 579 nm for complex **1**, 460, 517 nm for complex **2**, 602, 627 nm for complex **3** and 595 nm for complex **4**. Like PL spectra in solution, the emission spectra of complexes **2** and **3** in neat film also exhibit vibronically

Table 2
Calculated energy levels of the frontier molecular orbitals and HLG values of the four complexes in acetonitrile. All energies are given in eV.

Complex	HOMO	LUMO[a]	HLG
1	−5.72	−3.06	2.66
2	−6.04	−3.13	2.91
3	−5.69	−3.06	2.63
4	−5.73	−3.06	2.67

[a] The LUMO level was taken from the sum of the HOMO level and the TDDFT transition energy.

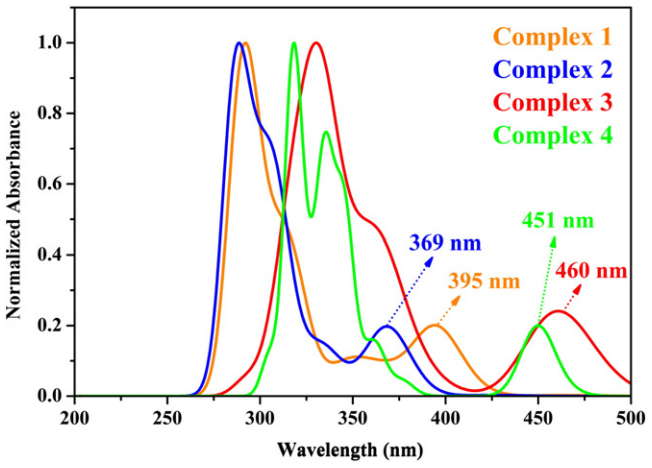

Fig. 4. Simulated UV–visible absorption spectra of the four complexes obtained at the B3LYP/6-31G(d,p)/LanL2DZ level of theory.

Table 3
Simulated absorption wavelengths (λ_{cal}), oscillator strengths (f), and coefficients of configuration interaction (CI) with the dominant contribution to each transition for the four complexes. The calculated emission wavelengths ($\lambda_{emission}$) are obtained by the ΔSCF method. H and L denote HOMO and LUMO, respectively.

Complex	Transition	λ_{cal} (nm)	f	CI coefficient	Dominant contribution (%)	$\lambda_{emission}$ (nm)
1	$S_0 \rightarrow S_1$	467	0.0008	0.7036	H → L (99)	582
	$S_0 \rightarrow S_2$	395	0.0603	0.6963	H → L + 1 (97)	
	$S_0 \rightarrow S_3$	380	0.0003	0.6908	H → L + 2 (95)	
	$S_0 \rightarrow S_4$	368	0.0130	0.6598	H − 1 → L (87)	
	$S_0 \rightarrow S_5$	363	0.0074	0.6110	H-2 → L (75)	
2	$S_0 \rightarrow S_1$	426	0.0009	0.7021	H → L (99)	565
	$S_0 \rightarrow S_2$	369	0.0572	0.6917	H → L + 1 (96)	
	$S_0 \rightarrow S_3$	361	0.0058	0.6743	H-1 → L (91)	
	$S_0 \rightarrow S_4$	356	0.0022	0.6788	H → L + 2 (92)	
	$S_0 \rightarrow S_5$	351	0.0033	0.6037	H-2 → L (73)	
3	$S_0 \rightarrow S_1$	471	0.0104	0.7021	H → L (99)	592
	$S_0 \rightarrow S_2$	460	0.0881	0.6985	H → L + 1 (98)	
	$S_0 \rightarrow S_3$	433	0.0008	0.6968	H → L + 2 (97)	
	$S_0 \rightarrow S_4$	393	0.0113	0.6932	H-1 → L (96)	
	$S_0 \rightarrow S_5$	381	0.0064	0.6701	H-2 → L (90)	
4	$S_0 \rightarrow S_1$	464	0.0041	0.6878	H → L (95)	571
	$S_0 \rightarrow S_2$	451	0.0546	0.5117	H → L + 1 (52)	
	$S_0 \rightarrow S_3$	442	0.0102	0.4970	H → L + 2 (49)	
	$S_0 \rightarrow S_4$	377	0.0131	0.6737	H-1 → L (91)	
	$S_0 \rightarrow S_5$	363	0.0251	0.6259	H-1 → L + 1 (78)	

structured emission peaks, indicating similar emissive mechanism in both solution and film state and the emission has been assigned to LC $^3\pi$–π^* state. The red shift and broadened PL spectra with long tails extending to 850 nm are due to the strong intermolecular interactions in neat films than in the solution [49]. The PLQYs of neat films of complexes **1**–**4** were also measured and shown in Table 4. The PLQY values of complexes in neat films are 0.06, 0.05, 0.12, and 0.03 for complexes 1–4, respectively, which decreases significantly as compared to that in solution owing to the severe excited-state quenching in neat films [49].

3.4. Electrochemical properties

Cyclic voltammetry was used to investigate the electrochemical properties and energy levels of the complexes. Fig. 8 displays the cyclic voltammograms of complexes **1**–**4** with redox potentials reported relative to the 0.2 mM ferricenium/ferrocene (Fc^+/Fc) couple in 0.1 M tetrabutylammonium hexafluorophosphate ($TBAPF_6$) in acetonitrile. Electrochemical data are summarized in Table 4. All complexes show an irreversible oxidation process at potentials of 1.04, 1.36, 1.03, and 1.05 V for **1**, **2**, **3**, and **4**, respectively. It is assumed that the oxidation of metal ion in mononuclear biscyclometalated iridium complexes are reversible, analogous to the oxidation of Ir(III)—Ir(IV), whereas the

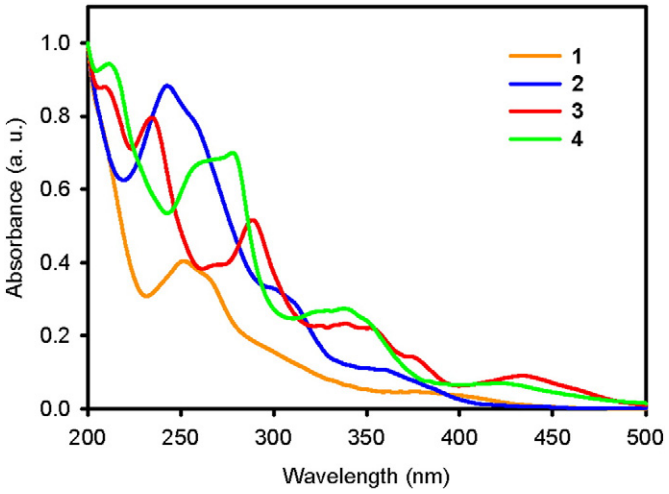

Fig. 5. UV–visible absorption spectra of cationic iridium complexes **1**–**4** in acetonitrile solution at room temperature.

irreversibility increases as the contribution to HOMO of the cyclometalating phenyl group increases [50]. Therefore, the irreversiblity in the oxidation process of complexes **1**–**4** could be attributed to σ—bond orbital due to one electron abstraction from $Ir(d_\pi)$—$\sigma(C^-)$ orbitals which in turn leads to dramatic weakening of Ir—C^- bond. It is noted that the oxidation potential of **2** is shifted in the positive direction by 330 mV, which indicates that complex **2** has a lower HOMO energy than the others due to the presence of electron-withdrawing fluorine atoms on the cyclometalating ligands. Besides, irreversible peaks observed at around 0.55 V are probably due to the presence of unavoidable impurities at electrode surfaces during electrochemical reaction. The complexes exhibit second oxidation waves at 1.39, 1.40, and 1.44 V for complexes 1, 3, and 4, respectively, which might be due to the oxidation of cyclometalated ligands. Irreversible reduction peaks are observed for all complexes at potentials of −1.77, −1.72, −1.62, and −1.63 V for complexes **1**, **2**, **3**, and **4**, respectively. From DFT calculations, it is confirmed that the reduction waves are due to reduction of the ancillary ligand with a slight contribution from the cyclometalating ligands. The reduction potential of Complex **3** is anodically shifted due to the electron donating nature of fused phenyl ring attached to pyridine moiety (isoquinoline moiety) that act to stabilize the LUMO and results narrower energy gap for **3** than complexes **1**, **2**, and **4**. In addition, all complexes **1**–**4** exhibit second reduction waves at −2.23, −2.18, −2.01, and −2.02 V, respectively, assigned to the reduction of cyclometalated ligands [51]. The HOMO and LUMO energies of complexes **1**–**4** were calculated from their

Table 4
Photophysical and electrochemical properties of cationic iridium complexes **1**–**4**.

Complex	UV λ_{abs} [a] [nm]	Room temperature emission							Electrochemical data [e]		
		PL λ_{max} [b] (nm)		Φ_p [c]		τ [d]	K_r ($\times 10^6$) s^{-1}	K_{nr} ($\times 10^7$) s^{-1}	E_{ox} [V]	E_{red} [V]	ΔE_{redox}
		CH_3CN	Film	CH_3CN	Film						
1	252, 266, 384, 406	575	579	0.09	0.06	34.63 ns	2.83	2.6	0.55 1.04 1.39	−1.77 −2.23	2.81
2	243, 255, 306, 362, 400	453, 487	460, 517	0.12	0.05	44 ns	2.69	2.0	0.54 1.36	−1.72 −2.18	3.08
3	210, 233, 269, 288, 353, 375, 436	589, 621	602, 627	0.31	0.12	0.51 μs	0.61	0.14	0.55 1.03 1.40	−1.62 −2.01	2.65
4	213, 260, 276, 340, 428	561	595	0.07	0.03	10.75 ns	6.61	8.64	0.60 1.05 1.44	−1.63 −2.02	2.68

[a] Absorbance measured in 1.0×10^{-5} M acetonitrile solution.
[b] Maximum emission wavelength, measured in acetonitrile solution at 1.0×10^{-5} M and in neat films.
[c] Φ_p was measured versus quinine sulfate ($\Phi_p = 0.545$ in 1 M H_2SO_4) and 9,10-diphenylanthracene ($\Phi_p = 0.90$ in cyclohexane).
[d] Excited state lifetime measured in acetonitrile solution along with calculated radiative and nonradiative decay rates.
[e] Measured in 1.0×10^{-3} M acetonitrile solution; potentials were quoted versus Fc^+/Fc (Fc is ferrocene).

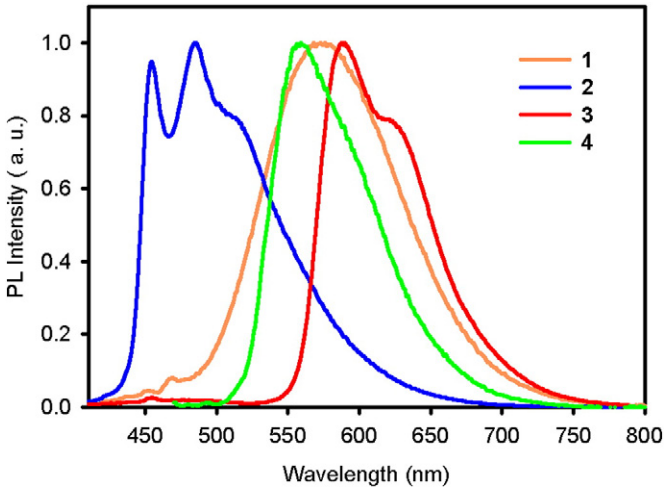

Fig. 6. Photoluminescence emission spectra of cationic iridium complexes **1–4** in acetonitrile.

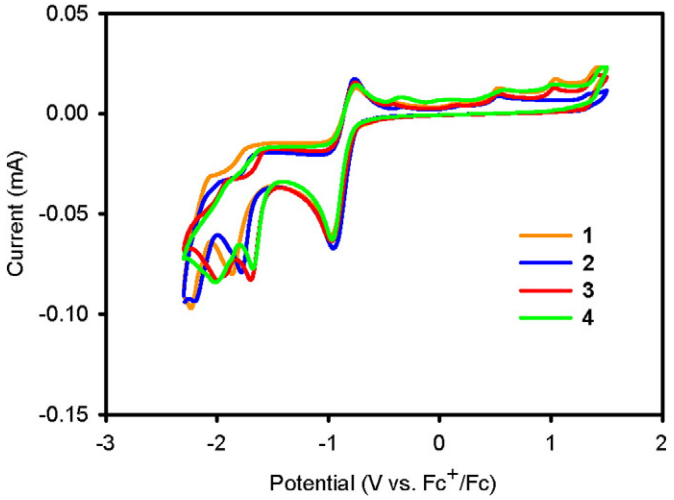

Fig. 8. Cyclic voltammograms of complexes **1–4**. Potentials are reported versus Fc^+/Fc (ferricenium/ferrocene).

corresponding oxidation and reduction potentials using the empirical relations given in the Experimental Section. The calculated HOMO energies are −5.41, −5.73, −5.40, and −5.42 eV, and the LUMO energies are −2.60, −2.65, −2.75, and −2.69 eV for complexes **1–4**, respectively. The electrochemical energy gaps ($E_{gap} = E_{HOMO} - E_{LUMO}$) of complexes **1–4** are 2.81, 3.08, 2.65, and 2.68 eV, respectively. The greater energy gap of **2** arises from stabilization of the HOMO and destabilization of the LUMO owing to the presence of electron-withdrawing fluorine atoms on the cyclometalating ligands.

4. Conclusions

A series of cationic iridium complexes with oxadiazole-based ancillary ligand have been synthesized and characterized through studies of their spectroscopic, photophysical, and electrochemical properties. The effect of different cyclometalating ligands on the optical properties of the complexes has been studied and compared. By appropriate selection of cyclometalating ligands, the photophysical properties of cationic iridium complexes in solution can be tuned from the yellow-orange to blue region of the visible spectrum. The PLQYs of the complexes have been measured which show a high quantum yield of 0.31 for complex **3** in acetonitrile solution. Use of the cyclometalating dfppy ligand in complex **2** resulted in an increased energy gap by HOMO stabilization, thereby shifting emission to the blue region. Density functional theory (DFT) and time-dependent DFT (TDDFT) calculations performed on complexes **1–4** corroborated the results of the photophysical and electrochemical experiments. This work has therefore established that the synthesized complexes with high PLQYs and good color tunability can be act as a promising material in LEC devices for solid-state lighting applications.

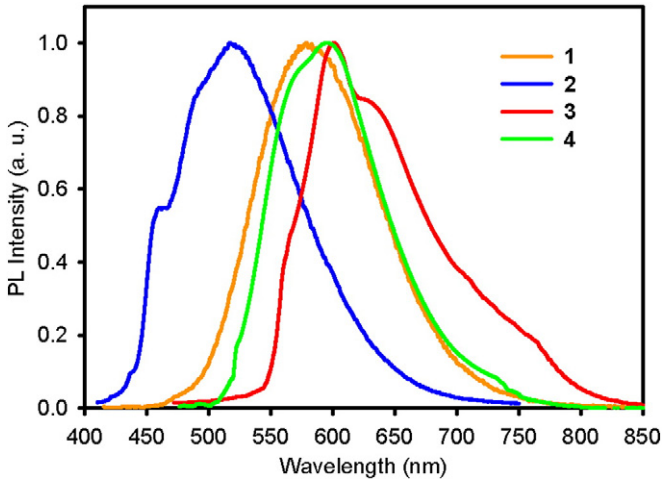

Fig. 7. Photoluminescence emission spectra of cationic iridium complexes **1–4** in neat films.

Acknowledgement

This research was supported by the National Research Foundation of Korea (NRF) funded by the Ministry of Science, ICT & Future Planning (No. NRF-2016R1D1A1B02013505) and the Brain Korea 21 Plus project.

Appendix A. Supplementary data

Supplementary data to this article can be found online at http://dx.doi.org/10.1016/j.jelechem.2016.09.037.

References

[1] R.D. Costa, E. Ortí, H.J. Bolink, F. Monti, G. Accorsi, N. Armaroli, Luminescent ionic transition-metal complexes for light-emitting electrochemical cells, Angew. Chem. Int. Ed. 51 (2012) 8178–8211.
[2] T. Hu, L. He, L. Duan, Y. Qiu, Solid-state light-emitting electrochemical cells based on ionic iridium(III) complexes, J. Mater. Chem. 22 (2012) 4206–4215.
[3] D.M. Schultz, T.P. Yoon, Solar synthesis: prospects in visible light photocatalysis, Science 343 (2014).
[4] Q. Zhao, C. Huang, F. Li, Phosphorescent heavy-metal complexes for bioimaging, Chem. Soc. Rev. 40 (2011) 2508–2524.
[5] J.-H. Yum, E. Baranoff, F. Kessler, T. Moehl, S. Ahmad, T. Bessho, A. Marchioro, E. Ghadiri, J.-E. Moser, C. Yi, M.K. Nazeeruddin, M. Grätzel, A cobalt complex redox shuttle for dye-sensitized solar cells with high open-circuit potentials, Nat. Commun. 3 (2012) 631.
[6] C.D. Sunesh, K. Shanmugasundaram, M.S. Subeesh, R.K. Chitumalla, J. Jang, Y. Choe, Blue and blue-green light-emitting cationic iridium complexes: synthesis, characterization, and optoelectronic properties, ACS Appl. Mater. Inter. 7 (2015) 7741–7751.
[7] C.D. Sunesh, Y. Choe, Synthesis and characterization of cationic iridium complexes for the fabrication of green and yellow light-emitting devices, Mater. Chem. Phys. 156 (2015) 206--213.
[8] C.D. Sunesh, M.S. Subeesh, K. Shanmugasundaram, R.K. Chitumalla, J. Jang, Y. Choe, Synthesis of heteroleptic iridium complexes with sterically hindered methyl groups on pyrazole ligands for efficient yellow and green light-emitting electrochemical cells, Dyes Pigments 128 (2016) 190–200.
[9] J.D. Slinker, A.A. Gorodetsky, M.S. Lowry, J. Wang, S. Parker, R. Rohl, S. Bernhard, G.G. Malliaras, Efficient yellow electroluminescence from a single layer of a cyclometalated iridium complex, J. Am. Chem. Soc. 126 (2004) 2763–2767.
[10] K.-Y. Lu, H.-H. Chou, C.-H. Hsieh, Y.-H.O. Yang, H.-R. Tsai, H.-Y. Tsai, L.-C. Hsu, C.-Y. Chen, I.C. Chen, C.-H. Cheng, Wide-range color tuning of iridium biscarbene complexes from blue to red by different N^N ligands: An alternative route for adjusting the emission colors, Adv. Mater. 23 (2011) 4933–4937.

[11] Q. Pei, G. Yu, C. Zhang, Y. Yang, A.J. Heeger, Polymer light-emitting electrochemical cells, Science 269 (1995) 1086–1088.
[12] J.D. Slinker, J.A. DeFranco, M.J. Jaquith, W.R. Silveira, Y.-W. Zhong, J.M. Moran-Mirabal, H.G. Craighead, H.D. Abruna, J.A. Marohn, G.G. Malliaras, Direct measurement of the electric-field distribution in a light-emitting electrochemical cell, Nat. Mater. 6 (2007) 894–899.
[13] H. Yersin, Triplet emitters for OLED applications, Mechanisms of Exciton Trapping and Control of Emission Properties, Transition METAL and Rare Earth Compounds: Excited States, Transitions, Interactions III, Springer Berlin Heidelberg, Berlin, Heidelberg 2004, pp. 1–26.
[14] M. Baldo, M. Segal, Phosphorescence as a probe of exciton formation and energy transfer in organic light emitting diodes, Phys. Status Solidi A 201 (2004) 1205–1214.
[15] Y. Fan, J. Zhao, Q. Yan, P.R. Chen, D. Zhao, Water-soluble triscyclometalated organoiridium complex: Phosphorescent nanoparticle formation, nonlinear optics, and application for cell imaging, ACS Appl. Mater. Interfaces 6 (2014) 3122–3131.
[16] M.-J. Li, P. Jiao, M. Lin, W. He, G.-N. Chen, X. Chen, High electrochemiluminescence of a new water-soluble iridium(iii) complex for determination of antibiotics, Analyst 136 (2011) 205–210.
[17] J. Slinker, D. Bernards, P.L. Houston, H.D. Abruna, S. Bernhard, G.G. Malliaras, Solid-state electroluminescent devices based on transition metal complexes, Chem. Commun. 2392–2399 (2003).
[18] P. Matyba, K. Maturova, M. Kemerink, N.D. Robinson, L. Edman, The dynamic organic p–n junction, Nat. Mater. 8 (2009) 672–676.
[19] C.D. Sunesh, G. Mathai, Y. Choe, Green and blue–green light-emitting electrochemical cells based on cationic iridium complexes with 2-(4-ethyl-2-pyridyl)-1H-imidazole ancillary ligand, Org. Electron. 15 (2014) 667–674.
[20] C.D. Sunesh, G. Mathai, Y. Choe, Constructive effects of long alkyl chains on the electroluminescent properties of cationic iridium complex-based light-emitting electrochemical cells, ACS Appl. Mater. Interfaces 6 (2014) 17416–17425.
[21] C.D. Sunesh, S. Ok, G. Mathai, Y. Choe, Electroluminescent properties of yellow light-emitting electrochemical cells based on a cationic iridium complex and the effect of ionic liquids incorporation in an active layer, Thin Solid Films 531 (2013) 530–534.
[22] C.D. Sunesh, G. Mathai, Y.-R. Cho, Y. Choe, Optoelectronic properties of green and yellow light-emitting electrochemical cells based on cationic iridium complexes, Polyhedron 57 (2013) 77–82.
[23] L. He, L. Duan, J. Qiao, G. Dong, L. Wang, Y. Qiu, Highly efficient blue-green and white light-emitting electrochemical cells based on a cationic iridium complex with a bulky side group, Chem. Mater. 22 (2010) 3535–3542.
[24] R.D. Costa, E. Ortí, H.J. Bolink, S. Graber, C.E. Housecroft, E.C. Constable, Intramolecular π-stacking in a phenylpyrazole-based iridium complex and its use in light-emitting electrochemical cells, J. Am. Chem. Soc. 132 (2010) 5978–5980.
[25] S. Graber, K. Doyle, M. Neuburger, C.E. Housecroft, E.C. Constable, R.D. Costa, E. Ortí, D. Repetto, H.J. Bolink, A Supramolecularly-caged ionic iridium(III) complex yielding bright and very stable solid-state light-emitting electrochemical cells, J. Am. Chem. Soc. 130 (2008) 14944–14945.
[26] H.C. Su, F.C. Fang, T.Y. Hwu, H.H. Hsieh, H.F. Chen, G.H. Lee, S.M. Peng, K.T. Wong, C.C. Wu, Highly efficient orange and green solid-state light-emitting electrochemical cells based on cationic IrIII complexes with enhanced steric hindrance, Adv. Funct. Mater. 17 (2007) 1019–1027.
[27] L. He, J. Qiao, L. Duan, G. Dong, D. Zhang, L. Wang, Y. Qiu, Toward highly efficient solid-state white light-emitting electrochemical cells: blue-green to red emitting cationic iridium complexes with imidazole-type ancillary ligands, Adv. Funct. Mater. 19 (2009) 2950–2960.
[28] H.J. Bolink, L. Cappelli, S. Cheylan, E. Coronado, R.D. Costa, N. Lardies, M.K. Nazeeruddin, E. Orti, Origin of the large spectral shift in electroluminescence in a blue light emitting cationic iridium(III) complex, J. Mater. Chem. 17 (2007) 5032–5041.
[29] Y. Liu, M.S. Liu, A.K.Y. Jen, Synthesis and characterization of a novel and highly efficient light-emitting polymer, Acta Polym. 50 (1999) 105–108.
[30] S.-W. Hwang, Y. Chen, Synthesis and electrochemical and optical properties of novel poly(aryl ether)s with isolated carbazole and p-quaterphenyl chromophores, Macromolecules 34 (2001) 2981–2986.
[31] M. Nonoyama, Benzo[*h*]quinolin-10-yl-N iridium(III) complexes, Bull. Chem. Soc. Japan. 47 (1974) 767–768.
[32] M.J. Frisch, G.W. Trucks, H.B. Schlegel, G.E. Scuseria, M.A. Robb, J.R. Cheeseman, G. Scalmani, V. Barone, B. Mennucci, G.A. Petersson, H. Nakatsuji, M. Caricato, X. Li, H.P. Hratchian, A.F. Izmaylov, J. Bloino, G. Zheng, J.L. Sonnenberg, M. Hada, M. Ehara, K. Toyota, R. Fukuda, J. Hasegawa, M. Ishida, T. Nakajima, Y. Honda, O. Kitao, H. Nakai, T. Vreven, J.A. Montgomery, J.E. Peralta, F. Ogliaro, M. Bearpark, J.J. Heyd, E. Brothers, K.N. Kudin, V.N. Staroverov, R. Kobayashi, J. Normand, K. Raghavachari, A. Rendell, J.C. Burant, S.S. Iyengar, J. Tomasi, M. Cossi, N. Rega, J.M. Millam, M. Klene, J.E. Knox, J.B. Cross, V. Bakken, C. Adamo, J. Jaramillo, R. Gomperts, R.E. Stratmann, O. Yazyev, A.J. Austin, R. Cammi, C. Pomelli, J.W. Ochterski, R.L. Martin, K. Morokuma, V.G. Zakrzewski, G.A. Voth, P. Salvador, J.J. Dannenberg, S. Dapprich, A.D. Daniels Farkas, J.B. Foresman, J.V. Ortiz, J. Ceioslowski, D.J. Fox, Gaussian 09, Revision B.01, Wallingford CT, 2009.
[33] A.D. Becke, Density-functional thermochemistry. III. The role of exact exchange, J. Chem. Phys. 98 (1993) 5648–5652.
[34] A.D. Becke, Density-functional thermochemistry. IV. A new dynamical correlation functional and implications for exact-exchange mixing, J. Chem. Phys. 104 (1996) 1040–1046.
[35] C. Lee, W. Yang, R.G. Parr, Development of the Colle-Salvetti correlation-energy formula into a functional of the electron density, Phys. Rev. B 37 (1988) 785–789.
[36] P.J. Hay, W.R. Wadt, Ab initio effective core potentials for molecular calculations. Potentials for the transition metal atoms Sc to Hg, J. Chem. Phys. 82 (1985) 270–283.
[37] P.J. Hay, W.R. Wadt, Ab initio effective core potentials for molecular calculations. Potentials for K to Au including the outermost core orbitals, J. Chem. Phys. 82 (1985) 299–310.
[38] W.R. Wadt, P.J. Hay, Ab initio effective core potentials for molecular calculations. Potentials for main group elements Na to Bi, J. Chem. Phys. 82 (1985) 284–298.
[39] S. Miertuš, E. Scrocco, J. Tomasi, Electrostatic interaction of a solute with a continuum. A direct utilizaion of AB initio molecular potentials for the prevision of solvent effects, Chem. Phys. 55 (1981) 117–129.
[40] M. Cossi, V. Barone, R. Cammi, J. Tomasi, Ab initio study of solvated molecules: A new implementation of the polarizable continuum model, Chem. Phys. Lett. 255 (1996) 327–335.
[41] R.K. Chitumalla, K.S.V. Gupta, C. Malapaka, R. Fallahpour, A. Islam, L. Han, B. Kotamarthi, S.P. Singh, Thiocyanate-free cyclometalated ruthenium(ii) sensitizers for DSSC: a combined experimental and theoretical investigation, Phys. Chem. Chem. Phys. 16 (2014) 2630–2640.
[42] D. Di Censo, S. Fantacci, F. De Angelis, C. Klein, N. Evans, K. Kalyanasundaram, H.J. Bolink, M. Grätzel, M.K. Nazeerudin, Synthesis, characterization, and DFT/TD-DFT calculations of highly phosphorescent blue light-emitting anionic iridium complexes, Inorg. Chem. 47 (2008) 980–989.
[43] S. Lamansky, P. Djurovich, D. Murphy, F. Abdel-Razzaq, H.-E. Lee, C. Adachi, P.E. Burrows, S.R. Forrest, M.E. Thompson, Highly phosphorescent bis-cyclometalated iridium complexes: synthesis, photophysical characterization, and use in organic light emitting diodes, J. Amer. Chem. Soc. 123 (2001) 4304–4312.
[44] S. Sprouse, K.A. King, P.J. Spellane, R.J. Watts, Photophysical effects of metal-carbon σ bonds in ortho-metalated complexes of Ir(III) and Rh(III), J. Amer. Chem. Soc. 106 (1984) 6647–6653.
[45] M.G. Colombo, T.C. Brunold, T. Riedener, H.U. Guedel, M. Fortsch, H.B. Buergi, Facial tris cyclometalated rhodium(3+) and iridium(3+) complexes: Their synthesis, structure, and optical spectroscopic properties, Inorg. Chem. 33 (1994) 545–550.
[46] M.G. Colombo, H.U. Guedel, Synthesis and high-resolution optical spectroscopy of bis[2-(2-thienyl)pyridinato-C3,N′](2,2′-bipyridine)iridium(III), Inorg. Chem. 32 (1993) 3081–3087.
[47] M.S. Lowry, W.R. Hudson, R.A. Pascal, S. Bernhard, Accelerated luminophore discovery through combinatorial synthesis, J. Am. Chem. Soc. 126 (2004) 14129–14135.
[48] A.B. Tamayo, S. Garon, T. Sajoto, P.I. Djurovich, I.M. Tsyba, R. Bau, M.E. Thompson, Cationic bis-cyclometalated iridium(III) diimine complexes and their use in efficient blue, green, and red electroluminescent devices, Inorg. Chem. 44 (2005) 8723–8732.
[49] L. He, L. Duan, J. Qiao, R. Wang, P. Wei, L. Wang, Y. Qiu, Blue-emitting cationic iridium complexes with 2-(1H-pyrazol-1-yl)pyridine as the ancillary ligand for efficient light-emitting electrochemical cells, Adv. Funct. Mater. 18 (2008) 2123–2131.
[50] G. Calogero, G. Giuffrida, S. Serroni, V. Ricevuto, S. Campagna, Absorption spectra, luminescence properties, and electrochemical behavior of cyclometalated iridium(III) and rhodium(III) complexes with a bis(pyridyl)triazole ligand, Inorg. Chem. 34 (1995) 541–545.
[51] Q. Zhao, S. Liu, M. Shi, C. Wang, M. Yu, L. Li, F. Li, T. Yi, C. Huang, Series of new cationic iridium(III) complexes with tunable emission wavelength and excited state properties: structures, theoretical calculations, and photophysical and electrochemical properties, Inorg. Chem. 45 (2006) 6152–6160.